Lamb–Mössbauer factor and second-order Doppler shift from inelastic nuclear resonant absorption

W. Sturhahn [a] and A. Chumakov [b]

[a] *Advanced Photon Source, Argonne National Laboratory, Argonne, IL 60439, USA*
[b] *European Synchrotron Radiation Facility, BP 220, F-38043 Grenoble, France*

The derivation of Lamb–Mössbauer factors and second-order Doppler shifts from data that are measured by inelastic nuclear resonant absorption of synchroton radiation is demonstrated. This approach offers a viable alternative to procedures that are based on elastic absorption and scattering techniques. The sources of error are evaluated, and a selection of examples is provided.

1. Introduction

The recoilless fraction or Lamb–Mössbauer factor and the second-order Doppler shift (SOD) are of general interest in Mössbauer spectroscopy. Both quantities strongly depend on the binding of the resonant nucleus in the lattice and vary with material composition, lattice structure, and environmental conditions, such as temperature or pressure. Also the Lamb–Mössbauer factor is closely related to the Debye–Waller factor, which is obtained from X-ray diffraction. In the past, Lamb–Mössbauer factors have been determined mostly by conventional Mössbauer transmission spectroscopy. In this approach, the accuracy depends on precise knowledge of the area density of the resonant nuclei. Determination of this area density turns out to be the dominant source for systematic errors due to, e.g., uncertainties in the sample geometry, isotopic abundance, or mass density of the sample. Moreover, knowledge of the Lamb–Mössbauer factor of the radioactive source is required. A logical approach to avoid the mix-up of source and absorber properties would be to replace the conventional radioactive source with an ideal one, for which the source parameters are well defined.

The proposal of Ruby [1] to substitute a radioactive source by a synchrotron radiation source for the excitation of nuclear levels was successfully realized by Gerdau et al. [2]. This pioneering experiment was followed by a variety of applications, which are summarized in [3]. A direct comparison of the sources was given by Sturhahn et al. [4]. The use of synchrotron radiation essentially eliminates errors related to source characteristics. However, the accurate determination of the Lamb–Mössbauer factor remains problematic [5–7] for the same reasons mentioned above, i.e., knowledge of the area density of the resonant nuclei is required. It is interesting to notice that self-absorption and related dynamical effects [8], which are usually considered a

complication in conventional Mössbauer transmission spectroscopy, now provide the means to obtain the Lamb–Mössbauer factor. On the other hand, the alteration of the source does not change the fact that the measured isomer shift is the sum of chemical isomer shift and SOD, rendering the two terms indistinguishable. The previously mentioned methods are based on elastic nuclear resonant absorption or scattering and therefore directly provide measurements of cross-sections under the constraint that the state of the lattice remains unchanged in the process. In this contribution, we will demonstrate that the Lamb–Mössbauer factor and SOD can be obtained by inelastic nuclear scattering techniques that require a change of the lattice state and may be interpreted as complementary to the traditional methods. However, the evaluation of the measured data is much more straightforward and precise and thus permits one to avoid many of the difficulties mentioned above.

Shortly after Mössbauer's famous discovery [9], theoretical work of Visscher [10] and Singwi and Sjölander [11] showed that nuclear resonant absorption can in principle provide information about lattice dynamics. It turned out that experiments of this kind require synchrotron radiation, as beautifully demonstrated by Seto et al. [12]. The quantitative analysis of such spectra including the extraction of the Lamb–Mössbauer factor, F, and the vibrational density of states (VDOS) was presented by Sturhahn et al. [13]. In contrast to the traditional methods, in which F is obtained directly (meaning that the measured signal disappears for $F = 0$), incoherent inelastic nuclear resonant absorption provides $1 - F$ [13,14]. Another significant merit of the new technique is that the SOD is obtained independently of chemical isomer shifts. The preferred approach is the observation of delayed atomic fluorescence of the resonant isotope versus the energy of incident X-rays from a pulsed synchrotron radiation beam [15]. This technique was called PHOENIX (PHOnon Excitation by Nuclear Inelastic absorption of X-rays) [16]. In the following sections, we explain how to derive the Lamb–Mössbauer factor and the SOD directly from the moments of the measured PHOENIX spectra. Proper normalization of these moments can be obtained without specific knowledge about isotopic abundance, shape or thickness of the sample, resonant cross-section, or hyperfine interactions. This property reduces systematic errors strongly. The residual sources for statistical and systematic errors inherent in the PHOENIX technique are discussed in a separate section. The technique does not distinguish different environments for the resonant isotope, and the measurement provides average values for the Lamb–Mössbauer factor and the SOD. The majority of PHOENIX experiments were conducted with the 14.413 keV resonance of the Mössbauer isotope ^{57}Fe because of the large resonance cross-section, the tolerable electronic absorption in the materials used, and the convenient lifetime. However, measurements using the 23.88 keV transition of ^{119}Sn [17–19] and the 21.542 keV transition of ^{151}Eu [20,21] were also reported. A comparison of the feasibility of experiments with various isotopes, which is based on eq. (2), is shown in table 1. The high intensity of third-generation synchrotron radiation sources, like the European Synchrotron Radiation Facility (ESRF), the Advanced Photon Source (APS), and the SPring-8, permits application of the PHOENIX technique even for unfavorable situations, e.g., when

Table 1
Isotopes with low energy resonances that are feasible for PHOENIX experiments. In the last column, the strength of the incoherent scattering channel is estimated. The values were obtained by calculating $\sigma_0\Gamma\eta_f\alpha_f/[(1+\alpha)\sigma_p]$ for each isotope, where σ_0 is the nuclear resonant cross-section, η_f is the fluorescence yield, α, α_f are the total and partial internal conversion coefficients, Γ is the nuclear level width, and σ_p is the photoelectric cross-section. The values were then normalized with respect to ^{57}Fe. For ^{83}Kr and ^{119}Sn, the fluorescence radiation is very soft, and its observation is not practical. In those cases, we substituted $\eta_f\alpha_f = 1$.

Isotope	Energy (keV)	Lifetime (ns)	Strength
^{169}Tm	8.410	5.8	0.22
^{83}Kr	9.4	212	0.062
^{57}Fe	14.413	141	1
^{151}Eu	21.54	14	0.37
^{119}Sn	23.88	25.7	3.9
^{161}Dy	25.66	40.5	0.53

small amounts of resonant nuclei are encountered such as in ultrathin films [22] or in proteins [23]. Consequently, accurate determination of Lamb–Mössbauer factors and SODs becomes possible for a much wider range of materials and sample conditions. As already mentioned, the Lamb–Mössbauer factor has a strong resemblance to the Debye–Waller factor, which is obtained from X-ray diffraction. In fact, the Lamb–Mössbauer factor and the Debye–Waller factor originate from the same expression under the conditions of "slow" and "fast" scattering, respectively. Nuclear resonant scattering is "slow" because the stages of absorption and emission are well separated on a time scale given by lattice dynamics. In the case of electronic charge scattering, absorption and emission occur almost instantaneously on this time scale, and the scattering process is "fast". For this reason, the Lamb–Mössbauer factor depends only on the momentum of the incident photon, **k**, whereas the Debye–Waller factor shows the same functional dependence on the momentum transfer, **q**. In a harmonic lattice, we obtain the relationship

$$\ln F_{\mathrm{DW}} = \frac{q^2}{k^2} \ln F_{\mathrm{LM}}, \tag{1}$$

where we assumed that **k** and **q** point in the same direction. The previous relation emphasizes the usefulness of Lamb–Mössbauer factors in related areas of science.

2. Sum rules

The main features of the typical PHOENIX spectrum are an elastic peak and side bands at lower and higher energy. For materials with reasonable probability for recoilless absorption, the elastic peak dominates the spectrum. In [13], the cross-

section for inelastic incoherent nuclear resonant absorption accompanied by emission of delayed atomic K-fluorescence is described by

$$\sigma(\mathbf{k}, E) = \sigma_0 \, \frac{\eta_\mathrm{f} \alpha_\mathrm{f}}{1+\alpha} \, \frac{\pi}{2} \, \Gamma \, S(\mathbf{k}, E), \tag{2}$$

where σ_0 is the nuclear resonant cross-section, η_f is the fluorescence yield, α, α_f are the total and partial internal conversion coefficients, and Γ is the nuclear level width. $\mathbf{k}$ is the wave vector of the incident radiation. The absorption probability per unit of energy, $S(\mathbf{k}, E)$, is given by the self-correlation of the atomic motion

$$S(\mathbf{k}, E) = \frac{1}{2\pi} \, \Re \int_0^\infty \mathrm{e}^{\mathrm{i}\omega t} \, \mathrm{e}^{-\Lambda t} L(\mathbf{k}, t) \, \mathrm{d}t, \tag{3}$$

where we used $E = \hbar\omega$ and $\Gamma = 2\hbar\Lambda$. $L(\mathbf{k}, t)$ is equivalent to the spatial Fourier transform of van Hove's self-correlation function $G_s(\mathbf{x}, t)$ [24, eq. (15)]

$$L(\mathbf{k}, t) = \left\langle \mathrm{e}^{-\mathrm{i}\mathbf{k}\cdot\hat{\mathbf{r}}(t)} \, \mathrm{e}^{\mathrm{i}\mathbf{k}\cdot\hat{\mathbf{r}}(0)} \right\rangle, \tag{4}$$

where $\hat{\mathbf{r}}$ is the displacement operator of the atom in Heisenberg representation. The dependence of $S(\mathbf{k}, E)$ on the direction of the incident photon is dicussed by Kohn et al. [25] for the case of anisotropic single crystals and by Sturhahn and Kohn [26] for the general case of a harmonic lattice. In the following, we will not explicitly write the $\mathbf{k}$-dependence unless needed. These expressions are relevant to this paper because they relate to the moments $S_n = \int E^n S(E) \, \mathrm{d}E$. However, straightforward calculation of S_n from eq. (3) fails for the even moments with $n \geqslant 2$ where we observe singular behavior. A regularization by using a proper cut-off for the integration range is justified because, in principle, eq. (3) requires modification for transient effects at very short times. Therefore it will be our understanding that energy integrations are properly cut off, and we obtain the useful relationship

$$S_n = (-\mathrm{i})^n \left(\frac{\mathrm{d}^n}{\mathrm{d}t^n} \, L(t) \right)_{t=0}. \tag{5}$$

Similar expressions were discussed by Lipkin [27] and provide a set of sum rules with a wide range of applicability.

The spectral shape that is obtained experimentally relates to the previous expressions by

$$I(E) = \int R\big(E - E'\big) \big\{ A S\big(E'\big) - B \delta\big(E'\big) \big\} \, \mathrm{d}E', \tag{6}$$

where E is the energy of the incident synchrotron radiation relative to the nuclear transition energy, $S(E) \, \mathrm{d}E$ is the probability for a vibrational excitation within the interval $[E, E + \mathrm{d}E]$ from eq. (3), and $R(E)$ is the normalized instrumental resolution function. The coefficients A and B depend on the experimental conditions. In particular, A provides the data normalization, and its precise determination is crucial to the data evaluation procedure. The coefficient B quantifies saturation effects that occur in the vicinity of the nuclear resonance, i.e., around $E = 0$. It serves to restore

the proper height of the central elastic peak; however, it does not affect the further calculations. After integration of eq. (6) we obtain

$$A = \frac{1}{E_R}\{I_1 - I_0 R_1\}, \qquad B = A - I_0, \tag{7}$$

where the moments $R_j = \int E^j R(E)\,\mathrm{d}E$ and $I_j = \int E^j I(E)\,\mathrm{d}E$ were introduced, and we made use of the sum rule $S_1 = E_R$, the recoil energy of the free nucleus. With these relations we obtain the appropriately normalized, convoluted excitation probability density

$$\int R\big(E - E'\big) S\big(E'\big)\,\mathrm{d}E' = \frac{1}{A}\big\{I(E) + BR(E)\big\}. \tag{8}$$

The values of A and B, however, provide insufficient knowledge for a determination of the probability for recoilless absorption, the Lamb–Mössbauer factor. In addition, we have to remove the elastic peak from the measured spectrum by some appropriate procedure. We obtain for the Lamb–Mössbauer factor

$$F = 1 - \frac{1}{A}\int I'(E)\,\mathrm{d}E, \tag{9}$$

where $I'(E)$ represents the measured spectrum after removal of the elastic peak, i.e., $I'(E) = I(E) - CR(E)$, $C > 0$. If the resolution function of the instrument, $R(E)$, was measured independently, e.g., in a setup using nuclear forward scattering; its shape can be fitted to the elastic peak in the PHOENIX spectrum to obtain a value for C. This procedure will work accurately if the energy dependence of the inelastic contribution under the elastic peak is known. Because elastic peaks occur only in solid materials, the use of a Debye model to approximate the inelastic contribution for small energies was suggested [28]. This approximation may be improved if the sound velocity of the material is known [25]. If the Lamb–Mössbauer factor is small, the multiphonon contribution at small energies increases strongly [18] and the removal of the elastic peak becomes difficult. If the determination of the elastic contribution fails, eq. (9) still provides a lower bound for the Lamb–Mössbauer factor, i.e., with $C = 0$ there follows $F \geqslant B/A$.

As shown in [13], the VDOS can be obtained from the PHOENIX spectra. The Lamb–Mössbauer factor can then be calculated from the VDOS to examine the reliability of the value that was obtained from the moments. Such an investigation was performed for iron metal (bcc) [28]. Furthermore, the Lamb–Mössbauer factor can be extrapolated to zero temperature [13,29].

Other moments of the probability density $S(E)$ provide valuable information about the vibrational behavior of the material. We can obtain this information from PHOENIX spectra after a relationship between those moments and the measured data

has been established. Under the assumption that the moments of the resolution function $R_j = \int E^j R(E)\,\mathrm{d}E$ exist for $0 \leqslant j \leqslant n$, we obtain the relationship [30]

$$I_n = A \sum_{j=0}^{n} \binom{n}{j} S_j R_{n-j} - B R_n. \tag{10}$$

This equation permits one to calculate the moments S_j recursively, e.g., for $n = 0$, 1 we recover eq. (7), and for the second moment there follows

$$S_2 = \frac{I_2}{A} - 2E_R R_1 - \frac{I_0}{A} R_2. \tag{11}$$

We want to emphasize that the extraction of the moments according to eq. (10) does not require the removal of the elastic peak and thus avoids the related difficulties. The second moment, S_2, provides the average kinetic energy of the nucleus projected onto the direction of the incident X-rays. The atomic vibrations are nonrelativistic, and we can write

$$S_2 = E_0^2 \frac{\langle (\hat{\mathbf{v}} \cdot \mathbf{k})^2 \rangle}{c^2 k^2} + E_R^2, \tag{12}$$

where $\hat{\mathbf{v}}$ is the velocity operator of the atom, E_0 is the nuclear transition energy, and $\langle\,\rangle$ denotes the ensemble average. The SOD is then obtained from measurements with the direction of the incident radiation along orthogonal axes:

$$\delta_{\mathrm{SOD}} = -E_0 \frac{\langle \hat{\mathbf{v}}^2 \rangle}{2c^2} = -\frac{S_{2x} + S_{2y} + S_{2z} - 3E_R^2}{2E_0}. \tag{13}$$

At this point it should be mentioned that the derivations of Lipkin [27] leading to our relationships between the PHOENIX spectra and Lamb–Mössbauer factor and SOD are merely based on the assumption that $\langle \hat{\mathbf{v}} \cdot \mathbf{k} \rangle = 0$ for the individual nuclei, which is generally the case in bound systems. No vibrational model was necessary to obtain the relationships.

In addition to the Lamb–Mössbauer factor and SOD, which were calculated from 0th-order, 1st-order and 2nd-order moments of the data and resolution function, the third moment S_3 provides an average force constant $D(\mathbf{k})$ projected onto the direction of the incident X-rays:

$$D(\mathbf{k}) = \frac{E_0^2}{2\hbar^2 c^2 E_R^2} \left\{ S_3(\mathbf{k}) - 3E_R S_2(\mathbf{k}) + 2E_R^3 \right\}. \tag{14}$$

This quantity is directly related to the binding strength of the resonant isotope. In a harmonic lattice, $D(\mathbf{k})$ is independent of temperature.

3. Accuracy of the method

In the previous sections, we explained the principles of obtaining the Lamb–Mössbauer factor and SOD from PHOENIX spectra. Practical applications will also require

quantitative estimates of statistical and systematic uncertainties. We will include the following sources of error in our discussion:

- normalization of measured spectra,
- derivation of the energy scale,
- detector noise,
- removal of the elastic peak.

The experimental procedure provides a set of data pairs $\{E_j, N_j\}$, i.e., at a certain energy of the incident radiation, E_j, a certain number of events, N_j, is registered. The values of N_j have unavoidable statistical uncertainties as well as errors related to the normalization procedure during data acquisition, e.g., counting at each energy for a fixed time period. Fluctuations of the incident intensity or other perturbations are then described by a normalization function $1 + \phi[E]$, and the potential systematic error is given by $\phi_j\, N_j$. At present, it is not difficult to achieve $|\phi_j| < 2\%$.

The energy of the incident radiation is a derived quantity, i.e., angle positions of monochromator crystals are converted to energy. The uncertainty of the angle measurement depends on the quality of the instrumentation as well as the accuracy of the crystal alignment [31–34]. The material properties and the temperatures of the monochromator crystals provide the angle–energy conversion. It is therefore important to monitor the crystal temperatures during data acquisition with mK sensivity and perform a corresponding correction [32]. The position of the elastic peak in the PHOENIX spectra determines the zero-energy of our energy scale. In summary, we will describe the energy calibration by

$$\psi[E] = E + \delta E_0 + \alpha\, E + \beta[E].$$

A perfect measurement would have no offset error, $\delta E_0 = 0$, perfect linear calibration, $\alpha = 0$, and vanishing nonlinearities $\beta[E] = 0$, i.e., $\psi[E] = E$. Realistic estimates are $|\delta E_0| < 0.1$ meV, $|\alpha| < 0.002$, $|\beta| < 0.1$ meV.

Detector background noise gives an energy-independent contribution to the spectrum. If determined independently, the measured data can be corrected. For the error in this procedure, δN_0, it is not difficult to obtain $\delta N_0 < 0.002\overline{N}$ with $\overline{N}$ being the average number of events.

The error that occurs when the elastic peak is removed from the measured data cannot be addressed generally. As described in the previous section, the procedure requires a model for the inelastic spectrum hidden under the elastic peak. If such a model is not available, the determination of the Lamb–Mössbauer factor according to eq. (9) may become very uncertain. However, the calculation of the higher moments derived from the PHOENIX spectrum is not affected.

We will now investigate the accuracy of the moments S_n using a simplified version of eq. (10). In this error analysis, we neglect contributions from the moments of the resolution function, R_n, $n > 0$. Note that by virtue of our normalization procedure

the uncertainty for S_1 vanishes. The relative uncertainties, δ_n, of the moments S_n are symbollically written as

$$\delta_n = \frac{I_1}{I_n}\,\delta\left[\frac{I_n}{I_1}\right]. \tag{15}$$

The actual calculation of the variation $\delta[\cdot]$ requires somes care due to the correlations between I_n and I_1, which originate from the same data. In a linear approximation, the range of relative errors is given by the minimum and maximum values of

$$\begin{aligned}\delta_n = &\sqrt{\frac{I_{2n}}{I_n^2} - 2\frac{I_{n+1}}{I_1 I_n} + \frac{I_2}{I_1^2}} + (n-1)\alpha + \delta E_0\left(n\,\frac{I_{n-1}}{I_n} - \frac{I_0}{I_1}\right)\\ &+ \sum_j N_j\,(\beta_j g_j)'\,\mathrm{d}E_j + \sum_j (\phi_j N_j + \delta N_0)\,g_j\,\mathrm{d}E_j,\end{aligned} \tag{16}$$

where $g_j = E_j^n/I_n - E_j/I_1$ and the prime denotes the derivative with respect to E_j. The first term reflects the statistical uncertainties caused by event counting and can be made arbitrarily small by increasing the data collection time. The next three terms account for the inaccuracy in the energy scale, and the last two terms describe errors from normalization and background determination. The uncertainty of the Lamb–Mössbauer factor is not accurately given by δ_0 because the error induced by removal of the elastic peak is not included. The correct range for the relative error of the Lamb–Mössbauer factor is obtained from

$$\delta_F = \frac{1-F}{F}\left(\delta_0' + \frac{\delta C}{I_0 - C}\right), \tag{17}$$

where δ_0' is calculated from eq. (16) by replacing $I_n \to I_n - C$, setting $n = 0$. The uncertainties in the removal of the elastic peak are expressed by δC with the value of C defined by eq. (9). The relative accuracy of the Lamb–Mössbauer factor increases as F approaches one. This arises from the fact that the described method actually measures the complement $1 - F$. Therefore, if F approaches values that are close to one, e.g., at low temperatures, we obtain particularly precise results.

We note that the various moments S_n of inelastic absorption, as well as the Lamb–Mössbauer factor, can alternatively be calculated from the vibrational density of states derived from the same data. Under most circumstances this may serve to verify the results and independently obtain an estimate for systematic errors [25].

4. Complex systems

In principle, the absorption probability density $S(\mathbf{k}, E)$ from eq. (3) can be different for each resonant nucleus in a given material. We accommodate this more general situation by a separate displacement operator $\hat{\mathbf{r}}_j$ for each nucleus in eq. (4). The PHOENIX spectra of such a system are then described by a linear superposition of the contributions of the individual nuclei because the underlying absorption process

is incoherent and correlations between the motion of different atoms are not observed. The latter property of the scattering process implies an average over all momentum transfers to the lattice and thus leads to a probability density per energy unit only [26]. If $S^{(j)}(\mathbf{k}, E)$ denotes the contribution of atom j, we may write

$$S(\mathbf{k}, E) = \frac{1}{N} \sum_{j=1}^{N} S^{(j)}(\mathbf{k}, E), \tag{18}$$

where N is the number of resonant nuclei. In practice, groups of resonant nuclei with identical excitation probability density are easily formed. Then it is more convenient to identify such a group of nuclei with an index j:

$$S(\mathbf{k}, E) = \sum_{j} a_j S^{(j)}(\mathbf{k}, E), \tag{19}$$

where a_j gives the probability of finding a resonant nucleus in this group. The coefficients satisfy $\sum_j a_j = 1$, $a_j \geqslant 0$, to maintain proper normalization. To demonstrate the consequences of many groups to the calculation of the Lamb–Mössbauer factor, we rewrite eq. (9) in terms of a function $S'(E)$ that differs from $S(E)$ only at $E = 0$, i.e., $S'(0) = 0$. We then use eq. (19) and the normalization for the coefficients a_j to obtain

$$F = \sum_{j} a_j \left\{ 1 - \int S^{(j)'}(E)\, \mathrm{d}E \right\}. \tag{20}$$

The term in braces represents the Lamb–Mössbauer factor of an individual group, and we find that the PHOENIX measurement provides a linear superposition. In general, all the moments of the data will be linear superpositions and the relationships that were outlined in the previous sections remain valid for the average values. The best way of dividing the nuclei into different groups depends on the particular case. For single crystals, each resonant nucleus per unit cell represents a group. In a homogeneous mixture of compounds, each compound containing resonant nuclei constitutes a group. For polycrystalline materials, which are a collection of randomly oriented small single crystals, the individual crystallites represent the groups. In the latter case, the averaged moments should be independent of the direction of the incident radiation.

Next, we consider the problem of extracting the concentrations of the individual compounds in a mixture. Mössbauer spectroscopy, conventional as well as with synchrotron radiation, usually provides the product of the concentration and the Lamb–Mössbauer factor for each constituent that is identified by the characteristic hyperfine splitting (fingerprinting technique). The concentrations can only be obtained after the Lamb–Mössbauer factors of the individual compounds have been measured. The determination of the Lamb–Mössbauer factor of the mixture alone is insufficient. Contrary to this technical problem, different lattice sites for the resonant nuclei in the unit cell pose a problem in principle. The local character of PHOENIX data does not permit one to make a distinction, and the measurement always provides the average over the unit cell. For iron borate ($FeBO_3$), e.g., the PHOENIX data clearly depend on the angle

between the 3-fold symmetry axis and the direction of the incident radiation [25,39], whereas for hematite (Fe_2O_3) no such behavior was observed [40]. Replacing every other iron atom in the hematite unit cell with boron essentially creates the iron borate unit cell. Therefore it was suggested that the different iron sites could produce PHOENIX spectra with opposite anisotropy such that cancellation occurs for hematite but not for iron borate [40]. A clear distinction of sites within the unit cell requires coherent scattering methods.

In the previous sections, we pointed out that the moments of the absorption probability density and the Lamb–Mössbauer factor could be calculated from the VDOS, which was obtained by a procedure outlined in [13]. This remains valid for the Lamb–Mössbauer factor even in the case of complex materials. On the other hand, the calculation of the moments and thus SOD and average force constant requires the true averaged VDOS. In general, the averaged absorption probability density, eq. (19), which is obtained by the PHOENIX method, does not lead to the true averaged VDOS, because the relationship between the absorption probability density and the VDOS is nonlinear. For clarification, we rewrite eqs. (5) of [13] for this case:

$$\begin{aligned} S^{(j)}(E) &= F^{(j)}\delta(E) + F^{(j)}\sum_{n=1}^{\infty} S_n^{(j)}(E), \\ S_1^{(j)}(E) &= \frac{E_R \mathcal{D}^{(j)}(E)}{E(1-\mathrm{e}^{-\beta E})}, \\ S_n^{(j)}(E) &= \frac{1}{n}\int S_{n-1}^{(j)}(E-\varepsilon) S_1^{(j)}(\varepsilon)\,\mathrm{d}\varepsilon, \quad n \geqslant 2. \end{aligned} \tag{21}$$

In this expression, $S_n^{(j)}(E)$ represents the n-phonon contribution to the excitation probability density of group j. β is the inverse temperature. This implicit equation for the true VDOS, $\mathcal{D}^{(j)}(E)$, can be inverted, e.g., by using the Fourier–Log method [42]. The averaged version of the previous equation is

$$S(E) = F\delta(E) + \sum_{n=1}^{\infty}\sum_{j} a_j F^{(j)} S_n^{(j)}(E). \tag{22}$$

In general, we cannot invert this expression to obtain the true average VDOS. At this point we note that a calculation of the moments of the absorption probability density using an approximated average VDOS need not result in the correct average moments even for perfectly harmonic lattices. Such comparisons can be helpful to distinguish different sites of the unit cell of a crystal [40].

5. Applications

So far, several experiments using inelastic nuclear resonant absorption provided values for the Lamb–Mössbauer factor and SOD or produced data relevant to such quantities. In figures 1 and 2, the Lamb–Mössbauer factors of iron metal (bcc) and

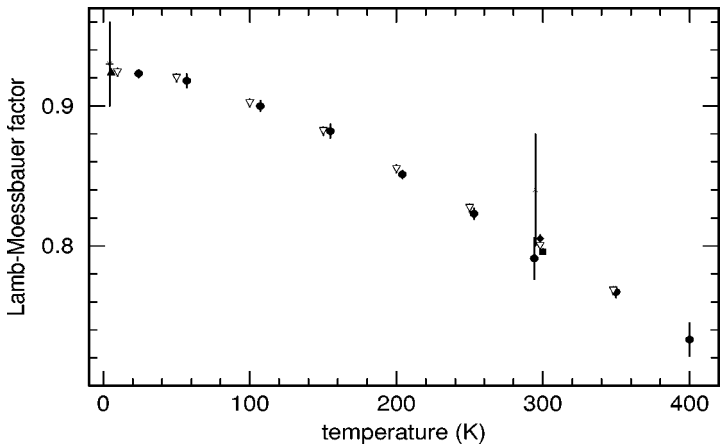

Figure 1. Lamb–Mössbauer factor of iron metal (bcc) versus temperature. The samples were polycrystalline iron foils at ambient pressure. The employed methods comprise Mössbauer spectroscopy ($\times$ – [43], $*$ – [44]), nuclear forward scattering ($\triangledown$ – [7]) and inelastic nuclear resonant absorption ($\blacklozenge$ – [13], $\bullet$ – [28], $\blacksquare$ – [32], $\blacktriangle$ – [38]).

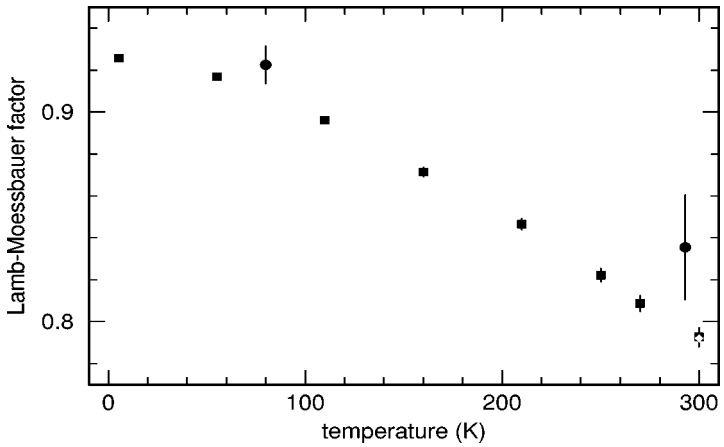

Figure 2. Lamb–Mössbauer factor of hematite (Fe_2O_3) versus temperature. The samples were either prepared from synthetic hematite powder [4,45] or single crystalline [40]. All data were taken at ambient pressure. Mössbauer spectroscopy($\bullet$ – [45]) and inelastic nuclear resonant absorption ($\blacksquare$ – [4], $\diamond$ – [40]) were used.

hematite (Fe_2O_3) are shown versus temperature, respectively. The uncertainties of the values obtained with the PHOENIX method are noticeably smaller. In the case of iron metal, the values obtained by the different experimental techniques show very good overall agreement. The data of [7] were normalized to $F = 0.924$ at 9.7 K to alleviate problems in the determination of the sample thickness in the original experiment [46]. The simple crystal structure of iron metal at normal pressure with one atom per irreducible unit does not cause problems related to distinguishable sites as

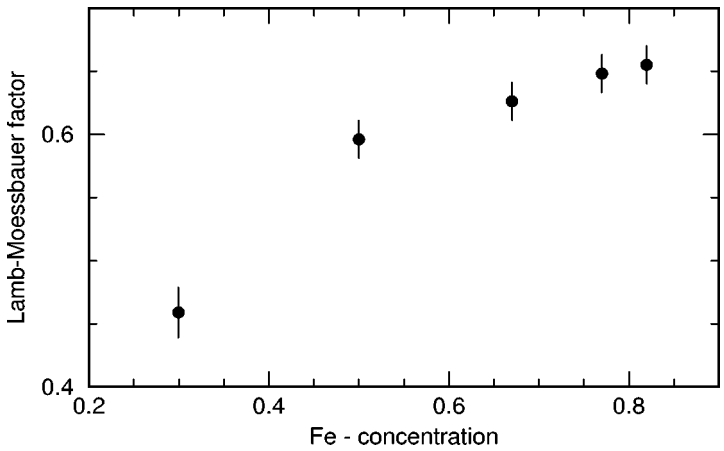

Figure 3. Lamb–Mössbauer factor of amorphous $Tb_{1-x}Fe_x$ films versus Fe-concentration. The thickness of the films was 17.5 nm. All measurements occurred at ambient conditions [22].

discussed in the previous section. For the hematite data larger differences are observed. In [45], the Lamb–Mössbauer factors were derived from the temperature dependence of the isomer shift. Problems related to this method were discussed earlier [47] and may explain the systematically larger values for F. In addition to providing reliable data in simple cases, the PHOENIX technique readily extends to systems that are difficult to investigate by other methods. Figure 3 shows the result of a series of measurements on amorphous $Tb_{1-x}Fe_x$ films with thicknesses of 17.5 nm [22]. In this particular case, the standard method of observing the temperature shift of the CEMS emission lines and then assigning a characteristic lattice temperature failed for low Fe-concentrations. Most likely unknown correlations between magnetic hyperfine fields and isomer shifts in the amorphous alloy caused these problems. However, the PHOENIX method is insensitive to the hyperfine interactions and can therefore provide reliable data. Table 2 contains values for the Lamb–Mössbauer factor for various compounds, including thin films and biological materials. In figures 4 and 5, the SODs of iron metal (bcc) and hematite (Fe_2O_3) are shown versus temperature. Such information is difficult to obtain from Mössbauer spectroscopy because chemical isomer shift and SOD are indistinguishable. As already mentioned, the PHOENIX method is not restricted to the resonant isotope ^{57}Fe. So far the ^{57}Fe, ^{119}Sn, and ^{151}Eu isotopes were used in PHOENIX experiments, which resulted in values for the Lamb–Mössbauer factor and SOD. In table 1, we listed a selection of candidates that have excitation energies below 30 keV. The latter restriction is mainly due to the difficulties to develop X-ray optics with sufficient energy resolution and efficiency for higher energies [34]. The estimate that is given in the last column of table 1 is based on eq. (2). Detector efficiencies were not considered. Also isotopes with a short lifetime of the Mössbauer level require extremely fast detectors, which at present poses a problem.

Table 2
Lamb–Mössbauer factor and SOD of various compunds. The values were obtained by inelastic nuclear resonant absorption using the PHOENIX method with ^{57}Fe, ^{119}Sn, or ^{151}Eu as resonant isotopes. All samples were measured under ambient conditions.

Compound	LM-factor	SOD (Γ)	Comments
Fe metal (bcc), foil	0.805(3)	−2.47(4)	[13]
	0.791(15)	−2.50(13)	[28]
	0.80(1)		[35]
	0.796(2)	−2.49(2)	[32]
Stainless steel, $Fe_{55}Cr_{25}Ni_{20}$, foil	0.742(10)	−2.41(4)	evaluated from [13]
	0.76(5)		[35]
Fe metal, nanocrystalline powder	0.726(15)	−2.62(12)	evaluated from [36]
Fe_3Al, foil	0.743(3)	−2.46(2)	evaluated from [37]
Pt_3Fe, foil	0.76(1)	−2.42(7)	[38]
Fe_2Tb, Laves phase, film	0.679(3)	−2.39(2)	[22]
$Fe_{67}Tb_{33}$, amorphous film	0.595(5)	−2.39(3)	[22]
$SrFeO_3$, powder	0.811(10)	−2.57(4)	evaluated from [13]
$SrFeO_{2.86}$, powder	0.814(10)	−2.60(4)	evaluated from [13]
$SrFeO_{2.74}$, powder	0.795(10)	−2.57(4)	evaluated from [13]
$SrFeO_{2.5}$, powder	0.640(15)	−2.54(4)	evaluated from [13]
$FeBO_3$, single crystal	0.81(3)		[39]
Fe_2O_3, powder	0.793(4)	−2.56(4)	[4]
Fe_2O_3, single crystal	0.792(5)	−2.58(6)	[40]
YIG, $Y_3Fe_5O_{12}$, single crystal	0.775(15)	−2.59(5)	[38]
$[Fe(bpp)_2][BF_4]$, polycrystalline	0.10(5)		[35]
metmyoglobin, wet powder	0.245(20)	−2.50(5)	[38]
SnO_2, powder	0.628(9)	−0.357(6)	[19]
$CaSnO_3$, powder	0.659(7)	−0.362(6)	[41]
SnO, powder	0.32(4)	−0.35(2)	[41]
V_3Sn, polycrystalline	0.40(4)	−0.34(3)	[41]
Nb_3Sn, polycrystalline	0.45(4)	−0.35(2)	[41]
Eu_2O_3, cubic phase, powder	0.590(13)	−0.045(1)	[21]

6. Conclusion

In this paper, the derivation of the Lamb–Mössbauer factor and the SOD from spectra of inelastic nuclear resonant absorption, the PHOENIX method, was demonstrated. We explained the application of sum rules that enable proper normalization of the raw data. Whereas the SOD is obtained from the moments of the data in a well-defined manner, the determination of the Lamb–Mössbauer factor requires the subtraction of the elastic peak in the PHOENIX spectrum. The latter procedure is usually realized by assuming a Debye-like behavior of the sample for small energies of vibrational excitation. We also discussed complex systems, i.e., mixtures of materials and different sites for the resonant nuclei in a crystallographic unit cell and concluded that the PHOENIX measurement provides a linear superposition. Further-

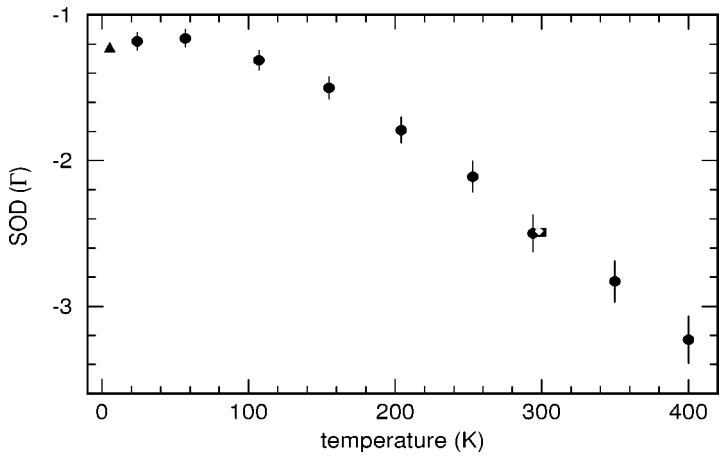

Figure 4. SOD of iron metal (bcc) versus temperature. The iron samples were polycrystalline foils. All measurements occured at ambient pressure. ◇ – [13], ● – [28], ■ – [32], ▲ – [38].

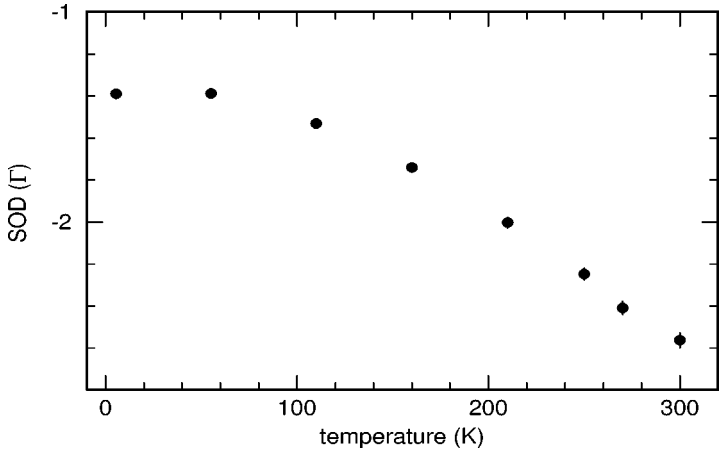

Figure 5. SOD of hematite (Fe_2O_3) versus temperature. Synthetic powder was used to prepare the Fe_2O_3 samples. All measurements occured at ambient pressure [4].

more, an account for realistic sources of systematic errors was provided. A collection of results from PHOENIX experiments that have been carried out so far clearly demonstrated the improved accuracy of the measured Lamb–Mössbauer factors. In the case of SODs, the results are unique. Our selection of examples implies the applicability of the PHOENIX method to a variety of sample types and the feasibility of measuring several Mössbauer isotopes.

Nuclear resonant scattering techniques like the PHOENIX method greatly benefitted from the integrated development of synchrotron radiation optics, detectors, and intense synchrotron radiation sources. The present paper illustrated one particular aspect of these points. Concerning future developments we suggest two topics. First, an

improvement of the energy resolution would directly affect the accuracy of the data and alleviate problems related to the removal of the elastic peak. At present energy resolutions of about 1 meV or slightly below are available [34]. Second, the properties of synchrotron radiation support efficient focusing. A small focal spot size would permit the investigation of very small amounts of material. In summary, it appears very likely that a continuing development of instruments and methods will further the potential of applications of nuclear resonant scattering with synchrotron radiation.

Acknowledgements

A.C. thanks his colleagues from the Nuclear Resonant Group at the ESRF for their help. W.S. is indebted to E.E. Alp, T.S. Toellner, P. Hession, M.Y. Hu, P. Lee and J. Sutter of SRI–CAT at the Advanced Photon Source for support during experiments. W.S. also thanks E.E. Alp and T.S. Toellner for fruitful discussions. Use of the Advanced Photon Source was supported by the U.S. Department of Energy, Basic Energy Sciences, Office of Energy research under Contract No. W-31-109-Eng-38.

References

[1] S.L. Ruby, J. de Physique 35 (1974) C6-209.
[2] E. Gerdau, R. Rüffer, H. Winkler, W. Tolksdorf, C.P. Klages and J.P. Hannon, Phys. Rev. Lett. 54 (1985) 835.
[3] E. Gerdau and H. de Waard, eds., *Nuclear Resonant Scattering of Synchrotron Radiation*, Hyp. Interact. 123–125 (1999/2000).
[4] W. Sturhahn, E.E. Alp, T.S. Toellner, P. Hession, M. Hu and J. Sutter, Hyp. Interact. 113 (1998) 47.
[5] E.E. Alp, T.M. Mooney, T. Toellner, W. Sturhahn, E. Witthoff, R. Röhlsberger, E. Gerdau, H. Homma and M. Kentjana, Phys. Rev. Lett. 70 (1993) 3351.
[6] W. Sturhahn and E. Gerdau, Phys. Rev. B 49 (1994) 9285.
[7] U. Bergmann, S.D. Shastri, D.P. Siddons, B.W. Battermann and J.B. Hastings, Phys. Rev. B 50 (1994) 5957.
[8] J.P. Hannon and G.T. Trammell, this issue, section III-1.2.
[9] R.L. Mößbauer, Z. Physik 151 (1958) 124.
[10] W.M. Visscher, Ann. Phys. 9 (1960) 194.
[11] K.S. Singwi and A. Sjölander, Phys. Rev. 120 (1960) 1093.
[12] M. Seto, Y. Yoda, S. Kikuta, X.W. Zhang and M. Ando, Phys. Rev. Lett. 74 (1995) 3828.
[13] W. Sturhahn, T.S. Toellner, E.E. Alp, X.W. Zhang, M. Ando, Y. Yoda, S. Kikuta, M. Seto, C.W. Kimball and B. Dabrowski, Phys. Rev. Lett. 74 (1995) 3832.
[14] A.I. Chumakov, R. Rüffer, H. Grünsteudel, H.F. Grünsteudel, G. Grübel, J. Metge and H.A. Goodwin, Europhys. Lett. 30 (1995) 427.
[15] A.I. Chumakov and W. Sturhahn, this issue, section V-1.1.
[16] W. Sturhahn, T.S. Toellner, K.W. Quast, R. Röhlsberger and E.E. Alp, Rev. Sc. Instr. 67(9) (1996) CD-ROM.
[17] S. Kikuta, Hyp. Interact. 90 (1994) 335.
[18] A.I. Chumakov, A. Barla, R. Rüffer, J. Metge, H.F. Grünsteudel, H. Grünsteudel, J. Plessel, H. Winkelmann and M.M. Abd-Elmeguid, Phys. Rev. B 58 (1998) 254.

[19] M.Y. Hu, T.S. Toellner, W. Sturhahn, P.M. Hession, J.P. Sutter and E.E. Alp, Nucl. Instrum. Methods A 430 (1999) 271.
[20] O. Leupold, University of Hamburg, private communication.
[21] P.M. Hession, W. Sturhahn, E.E. Alp, T.S. Toellner, M.Y. Hu, J.P. Sutter and J.G. Mullen, Argonne National Laboratory, in preparation.
[22] W. Keune and W. Sturhahn, this issue, section V-1.5.
[23] C. Keppler, K. Achterhold, A. Ostermann, U. van Bürck, W. Potzel, A.I. Chumakov, A.Q.R. Baron, R. Rüffer and F. Parak, Eur. Biophys. J. 25 (1997) 221.
[24] L. Van Hove, Phys. Rev. 95 (1954) 249.
[25] V.G. Kohn, A.I. Chumakov and R. Rüffer, Phys. Rev. B 58 (1998) 8437.
[26] W. Sturhahn and V.G. Kohn, this issue, section III-2.2.
[27] H.J. Lipkin, Ann. Phys. 9 (1960) 332; Phys. Rev. B 52 (1995) 10073.
[28] A.I. Chumakov, R. Rüffer, A.Q.R. Baron, H. Grünsteudel and H.F. Grünsteudel, Phys. Rev. B 54 (1996) R9596.
[29] A.I. Chumakov and R. Rüffer, Hyp. Interact. 113 (1998) 59.
[30] M.Y. Hu, W. Sturhahn, T.S. Toellner, P.M. Hession, J.P. Sutter and E.E. Alp, Nucl. Instrum. Methods A 428 (1999) 551.
[31] T.M. Mooney, T.S. Toellner, W. Sturhahn, E.E. Alp and S.D. Shastri, Nucl. Instrum. Methods A 347 (1994) 348.
[32] T.S. Toellner, M. Hu, W. Sturhahn, K.W. Quast and E.E. Alp, Appl. Phys. Lett. 71 (1997) 2112.
[33] A.I. Chumakov, R. Rüffer, A.Q.R. Baron, J. Metge, H. Grünsteudel and H.F. Grünsteudel, SPIE Proceedings 3151 (1997) 262.
[34] T.S. Toellner, this issue, section VI-1.
[35] A.I. Chumakov, J. Metge, A.Q.R. Baron, R. Rüffer, Yu.V. Shvyd'ko, H. Grünsteudel and H.F. Grünsteudel, Phys. Rev. B 56 (1997) R8455.
[36] B. Fultz, C.C. Ahn, E.E. Alp, W. Sturhahn and T.S. Toellner, Phys. Rev. Lett. 79 (1997) 937.
[37] B. Fultz, T.A. Stevens, W. Sturhahn, T.S. Toellner and E.E. Alp, Phys. Rev. Lett. 80 (1998) 3304.
[38] W. Sturhahn, Argonne National Laboratory, unpublished.
[39] A.I. Chumakov, R. Rüffer, A.Q.R. Baron, H. Grünsteudel, H.F. Grünsteudel and V.G. Kohn, Phys. Rev. B 56 (1997) 10758.
[40] P.M. Hession, W. Sturhahn, E.E. Alp, T.S. Toellner, P. Metcalf, M.Y. Hu, J.P. Sutter and J.G. Mullen, Argonne National Laboratory, in preparation.
[41] M.Y. Hu, Argonne National Laboratory, unpublished.
[42] D.W. Johnson and J.C.H. Spence, J. Phys. D: Appl. Phys. 7 (1974) 771.
[43] T.A. Kovats and J.C. Walker, Phys. Rev. 181 (1968) 610.
[44] H. Vogel, H. Spiering, W. Irler, U. Volland and G. Ritter, J. de Physique 40 (1979) C2-676.
[45] E. De Grave and A. van Alboom, Phys. Chem. Minerals 18 (1991) 337.
[46] S.D. Shastri, Argonne National Laboratory, private communication (August 1998).
[47] R.M. Housley and F. Hess, Phys. Rev. 146 (1966) 517.